

# Beyond Boolean: Ternary networks and dynamics

Cite as: Chaos 32, 083117 (2022); <https://doi.org/10.1063/5.0097874>

Submitted: 02 May 2022 • Accepted: 06 July 2022 • Published Online: 10 August 2022

 Yu-Xiang Yao,  Jia-Qi Dong, Jie-Ying Zhu, et al.



View Online



Export Citation



CrossMark

APL Machine Learning

Open, quality research for the networking communities

**Now Open for Submissions**

LEARN MORE

# Beyond Boolean: Ternary networks and dynamics

Cite as: Chaos 32, 083117 (2022); doi: 10.1063/5.0097874

Submitted: 2 May 2022 · Accepted: 6 July 2022 ·

Published Online: 10 August 2022



View Online



Export Citation



CrossMark

Yu-Xiang Yao,<sup>1,2</sup>  Jia-Qi Dong,<sup>1</sup>  Jie-Ying Zhu,<sup>2</sup> Liang Huang,<sup>1,a)</sup>  Duan-Qing Pei,<sup>3</sup>  and Ying-Cheng Lai<sup>4,5</sup> 

## AFFILIATIONS

<sup>1</sup>Lanzhou Center for Theoretical Physics and Key Laboratory of Theoretical Physics of Gansu Province, Lanzhou University, Lanzhou, Gansu 730000, China

<sup>2</sup>South China Institute for Stem Cell Biology and Regenerative Medicine, Guangzhou Institutes of Biomedicine and Health, Chinese Academy of Sciences, Guangzhou, Guangdong 510530, China

<sup>3</sup>Laboratory of Cell Fate Control, School of Life Sciences, Westlake University, Hangzhou, Zhejiang 310024, China

<sup>4</sup>School of Electrical, Computer and Energy Engineering, Arizona State University, Tempe, Arizona 85287, USA

<sup>5</sup>Department of Physics, Arizona State University, Tempe, Arizona 85287, USA

<sup>a)</sup> Author to whom correspondence should be addressed: [huangl@lzu.edu.cn](mailto:huangl@lzu.edu.cn)

## ABSTRACT

Boolean networks introduced by Kauffman, originally intended as a prototypical model for gaining insights into gene regulatory dynamics, have become a paradigm for understanding a variety of complex systems described by binary state variables. However, there are situations, e.g., in biology, where a binary state description of the underlying dynamical system is inadequate. We propose random ternary networks and investigate the general dynamical properties associated with the ternary discretization of the variables. We find that the ternary dynamics can be either ordered or disordered with a positive Lyapunov exponent, and the boundary between them in the parameter space can be determined analytically. A dynamical event that is key to determining the boundary is the emergence of an additional fixed point for which we provide numerical verification. We also find that the nodes playing a pivotal role in shaping the system dynamics have characteristically distinct behaviors in different regions of the parameter space, and, remarkably, the boundary between these regions coincides with that separating the ordered and disordered dynamics. Overall, our framework of ternary networks significantly broadens the classical Boolean paradigm by enabling a quantitative description of richer and more complex dynamical behaviors.

Published under an exclusive license by AIP Publishing. <https://doi.org/10.1063/5.0097874>

A celebrated paradigm in biological science is Boolean networks first articulated by Kauffman in 1969 as models of genetic regulatory networks. A Boolean network is a discrete-time dynamical system with a set of discrete state variables, where each variable is associated with a node in the network and a node takes inputs from a subset of nodes in the network to generate an output through a nonlinear Boolean function of the subset of input variables. The Boolean functions are node-dependent, and they determine the connectivity or the topology of the network. Given the state of the network at the present time, the Boolean functions determine the network state at the next time step, which can be done synchronously or asynchronously. Since their introduction more than 50 years ago, Boolean networks have become a paradigm not only in biology for gaining deep quantitative insights into the workings of gene regulatory networks and ecological systems, but also in a broad range of fields for understanding a variety of complex dynamical behaviors. Yet, in spite

of the great success of the Boolean network paradigm, there are situations, e.g., in biology, where a binary description is fundamentally inadequate, calling for the study of discrete-valued networked dynamical systems beyond the Boolean paradigm. Ternary networks, dynamical systems with three possible state values, have attracted some recent attention, but a general analysis of the dynamical properties of those networks is lacking. This article introduces a random ternary-network model and investigates issues, such as the emergence of ordered and disordered states, critical transitions, Lyapunov exponent, the nodes engaged in the dynamical processes, the associated scaling laws, and scalability. The phenomena are understood analytically and verified numerically. The ternary-network framework goes beyond the classical Boolean networks with significantly richer dynamical behaviors and represents a new “playground” to explore, understand, and exploit complex biological, physical, and social phenomena.

## I. INTRODUCTION

A paradigm enabling a quantitative description of many complex biological phenomena is random Boolean networks introduced by Kauffman<sup>1,2</sup> in 1969. Since then, these networks have been extended to other fields to investigate diverse dynamical behaviors, such as percolation,<sup>3</sup> evolution,<sup>4</sup> and even certain social phenomena.<sup>5,6</sup> A random Kauffman Boolean network consists of  $N$  nodes, where each node can be in one of two possible states: zero and one. The state of an individual node is determined by the signals from  $K$  randomly selected nodes in the network, which are fixed during the dynamical evolution. The mapping functions from these nodes are chosen randomly according to a global bias parameter  $p$ —the probability of a node in the state one. The statistical and dynamical behaviors of a Boolean network are thus determined by three parameters:  $(N, K, p)$ . In the past few decades, random Boolean networks have been studied to understand a variety of dynamical behaviors in complex systems, such as patterns, criticality, phase transitions, and stability.<sup>7–14</sup>

The core of Boolean dynamics is the updating rule; i.e., how the values of the nodes are updated at the next time step from the inputs at the current time step. In Kauffman's original formulation,<sup>1,2</sup> all nodes update their values synchronously, leading to synchronous Boolean networks. To accommodate more realistic circumstances, modified updating rules have been introduced, such as asynchronous, probabilistic, or threshold based strategies.<sup>15–17</sup> In spite of the astounding success of the classical Kauffman Boolean networks in describing and understanding a large variety of complex systems, there are situations where to adequately describe the dynamics requires modifications beyond improving the updating rules, such as making the network weighted or designating a new state to the system.<sup>18–20</sup> In fact, introducing additional dynamical states into the classical Boolean paradigm becomes necessary. In this regard, even the presence of a third state can potentially greatly expand the range of applicability of discrete-state dynamical systems as the resulting ternary network would naturally generate a much richer variety of dynamical behaviors beyond those enabled by the Boolean networks. Yet, in spite of some relevant works, such as the ternarization of musical rhythms,<sup>21</sup> sparse and ternary deep neural networks for efficient computation and memory,<sup>22–27</sup> there is little work in the current literature on the nonlinear dynamics of ternary networks, calling for a systematic study of these discrete-state dynamical networks.

In this paper, we generalize the classical Boolean networks to articulate a random network model with discrete ternary state variables and investigate the general dynamical properties of the resulting networks. Depending on the parameter values, a ternary network can deliver ordered stable dynamical behaviors, such as those corresponding to a fixed point or a short periodic orbit, or it can generate chaotic disordered states. We introduce a Hamming-distance based Lyapunov exponent to characterize the evolution between two nearby network state vectors, where a positive (negative) value of the exponent signifies disordered (ordered) dynamics. Another focus of our study is to identify the regions in the parameter space, which generate the ordered or disordered dynamics. Our main approach is to develop an analytic theory to quantitatively describe the boundaries separating the ordered and disordered regions. From the point of view of control and scalability, we find

that, when a disordered state emerges, the number of responsible nodes engaged in this process can be on the same order of magnitude as the system size, but a small fraction of nodes are already sufficient to generate a globally ordered state. An apparently abrupt increase in the number of nodes engaged in generating the global dynamical state in the network is thus a strong signature of the transition from an ordered to a disordered state, and this provides another criterion for determining the boundary between the two distinct types of states in the parameter space. Remarkably, at the critical transition point, the number of engaged nodes follows a scaling relation with the system size. Taken together, our ternary networks provide a framework that makes possible a quantitative description of richer and more complex dynamical behaviors beyond the classical Boolean paradigm.

## II. CLASSICAL KAUFFMAN BOOLEAN NETWORKS AND PROPOSED TERNARY GENERALIZATION

### A. Classical Kauffman Boolean networks

A classical Kauffman Boolean network is a directed network of  $N$  nodes, where each node receives inputs from  $K$  nodes selected randomly from the remaining  $N - 1$  nodes. There are thus two basic structural parameters:  $N$  and  $K$ ; therefore, the classical Kauffman model is also named as the  $N$ - $K$  model. In general, the set of  $K$  nodes that provide the signals to a node is fixed during the dynamical evolution of the network. The distribution of the in-degree  $k_{\text{in}}$ , i.e., the number of inputs for a node, can be written as  $P_{\text{in}}(k_{\text{in}}) = \delta_{k_{\text{in}}, K}$ , where  $\delta$  is the Kronecker symbol that returns one if  $k_{\text{in}} = K$  and zero otherwise. The distribution of the out-degree  $k_{\text{out}}$ , i.e., the number of outputs from a node, is Poisson,

$$P_{\text{out}}(k_{\text{out}}) = \frac{e^{-K} K^{k_{\text{out}}}}{k_{\text{out}}!},$$

with mean and variance  $K$ . The state of node  $i$  at time  $t + 1$ , denoted as  $s_i(t + 1)$ , is completely determined by its  $K$  inputs at time  $t$ ,

$$s_i(t + 1) = f_i(s_{i_1}(t), s_{i_2}(t), \dots, s_{i_K}(t)), \quad (1)$$

where  $f$  is the so-called Boolean mapping function, which acts as a mapping table  $\{0, 1\}^K \mapsto \{0, 1\}$ . The  $K$  input variables form  $2^K$  input patterns; therefore,  $2^{2^K}$  possible mapping functions can be assigned to the nodes, among which half will output a one and another half will yield a zero.

The third parameter in the Kauffman model is the bias  $p$ . Out of the  $2^{2^K}$  available mapping functions, half will yield one and the other half will yield zero. The bias  $p$  is the probability that a mapping function yielding one will be chosen. Thus, for  $p \neq 1/2$ , the  $2^{2^K}$  possible functions are not uniformly assigned to the nodes. The bias parameter  $p$ , the two basic structural parameters  $N$  and  $K$ , and the corresponding updating rules completely determine the dynamical evolution of the classical Kauffman Boolean network. In general, the statistical properties of the updating rules are controlled by the bias  $p$ , and all the nodes update their values simultaneously.<sup>1,2</sup> In the absence of noise or stochastic disturbances, the Kauffman network is a purely deterministic dynamical system. For any given initial state in the  $\{0, 1\}^N$  state space of size  $2^N$ , the trajectory is deterministic. Due to the finite size of the state space, a dynamical

trajectory approaches either a fixed point (a steady state) or a limit cycle exhibiting periodic oscillations. In the latter case, if the period is long, in any time interval that is much less than the period, the trajectory behaves as if it were disordered or chaotic—a situation that is common in the infinite system limit  $N \rightarrow \infty$ .

An issue concerning the two distinct dynamical states is their stability against random perturbations. For example, consider a binary vector of size  $N$  and its slightly perturbed version in which a few bits are different. Under the same updating rules, the difference can decay rapidly to zero or spread throughout the whole system, corresponding, respectively, to the state being stable or unstable. A convenient way to characterize the difference between two binary states is the normalized Hamming distance between the two states, which is the number of bits with different values normalized by the length  $N$  of the states,

$$d(\mathbf{s}_1, \mathbf{s}_2) = 1 - \frac{1}{N} \sum_i^N \delta_{s_{1i}, s_{2i}}, \quad (2)$$

where  $\mathbf{s}_1$  and  $\mathbf{s}_2$  are two states of length  $N$  and  $\delta_{s_{1i}, s_{2i}} = 1$  for  $s_{1i} = s_{2i}$  and zero otherwise. Note that the  $\delta$ -operation corresponds to the Not Exclusive OR (XNOR,  $\odot$ ) operator in the Boolean context. Typically, an initially nonzero distance  $d$  will either decay to zero or reach a finite value, where the former situation is an ordered/frozen phase while the latter corresponds to a disordered/chaotic phase.<sup>28,29</sup>

It is worth emphasizing that, because the state space is finite, a classical Kauffman network has no true chaos. Nonetheless, a short-term chaotic-like behavior can arise for a sufficiently long periodic orbit, especially for large systems. In fact, for both ordered and disordered states, the evolution of the separation between two nearby trajectories can be calculated in a finite time interval, leading to a quantity similar to the largest Lyapunov exponent for characterizing the nature of the trajectory, i.e., ordered or disordered.<sup>10</sup> Numerous previous studies<sup>7,9,10,12,28,30</sup> have established the critical condition under which a disordered phase can emerge:  $2p(1-p)K > 1$  in the large  $N$  limit. This provides a convenient criterion to determine if the dynamical state of a Kauffman network is ordered or disordered.

## B. Proposed ternary-network model

For a multi-valued discrete system, the state space is dramatically expanded from that of the classical two-state Boolean network. For example, if each node can have three distinct states, the total number of states will be  $3^N$ . An appealing feature of the Boolean networks, because of the binary states, is their natural correspondence to logic systems. For a ternary system, this correspondence no longer exists. As a result, the arithmetical operations in a conventional logic do not apply to a ternary system. For this reason, we denote the ternary values as  $\{\alpha, \beta, \gamma\}$  instead of  $\{1, 2, 3\}$ . For a ternary network of  $N$  nodes with  $K$  inputs to each node, the states can still be updated synchronously for all the nodes. The number of mapping functions for given  $K$  is now  $3^{3^K}$ . To characterize the probability for each ternary value to be generated, in general, requires two independent parameters. In particular, a bias parameter set  $(p, q, r)$  is required, where  $p(q, r)$  is the probability that the chosen mapping functions generate the value  $\alpha(\beta, \gamma)$ , where  $p + q + r = 1$ . Concepts in the classical Boolean systems, such as trajectory, Hamming

distance, fixed points, and limit cycles, can naturally be carried over into our ternary-network framework.

Simulation steps of the ternary-network dynamics are listed in Appendix A.

## III. RESULTS

### A. Phase diagram and transition between ordered and disordered dynamics for constrained biases

We first consider the special case of a constrained bias set given by  $(p, q, q)$  with  $q = (1-p)/2$ . In this case, the network dynamics are controlled by a single parameter,  $p$ , the probability that the value  $\alpha$  will be generated by choosing properly the mapping functions of the nodes. Similar to the classical Boolean model, the ternary system in this case has three parameters:  $(N, K, p)$ . Using the annealed approximation,<sup>7</sup> we derive the following iterative formula for the normalized Hamming distance  $d(t)$  between the two states:

$$d(t+1) = \frac{(1-p)(3p+1)}{2} \{1 - [1 - d(t)]^K\}. \quad (3)$$

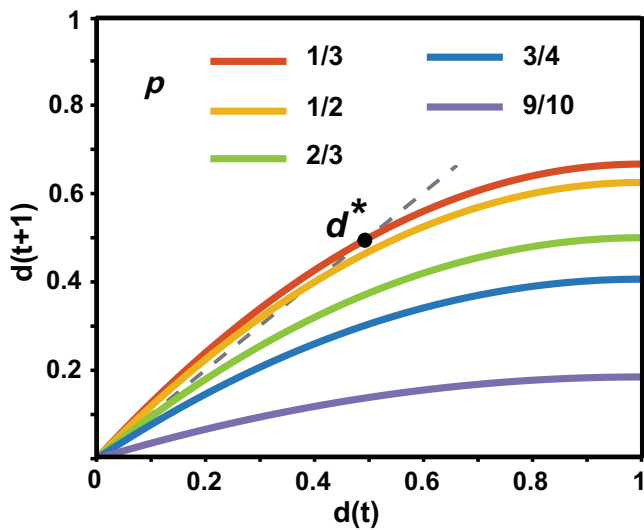
(A detailed derivation is presented in Appendix B.)

Figure 1 shows some representative mapping functions of  $d(t+1)$  vs  $d(t)$  for  $K = 2$  and a number of  $p$  values—the so-called Derrida curves.<sup>7</sup> These distance maps allow the dynamics of the Hamming distance to be analyzed. For example, the fixed point for the normalized Hamming distance, defined as  $d(t+1) = d(t)$ , can be determined by the intersection point of the Derrida curves with the line  $d(t+1) = d(t)$ . A fixed point will be stable if the absolute value of the slope is less than one; otherwise, it is unstable. Figure 1 indicates that, depending on the value of  $p$ , there can be either one or two fixed points. In particular, from Eq. (3), there is only one fixed point at 0 if  $dd(t+1)/dd(t)|_{d(t)=0} < 1$ , which yields

$$(1-p)(3p+1)K/2 < 1. \quad (4)$$

For  $K = 2$ , the condition becomes  $p > 2/3$ . In this case, zero is the only fixed point, and it is stable. As a result, a random initial perturbation will decay with time, leading to  $d(t) = 0$  [in which the two states  $\mathbf{s}_1(t)$  and  $\mathbf{s}_2(t)$  are identical]. As  $p$  decreases through  $p_c = 2/3$ , a tangent bifurcation occurs, after which two crossing points exist: zero and  $d^*$ . In this case, as shown by the curves of  $p = 1/3$  and  $p = 1/2$  in Fig. 1, the fixed point  $d(t) = 0$  is unstable, but  $d^*$  is stable. In the  $\mathbf{s}$  space, the two states  $\mathbf{s}_1(t)$  and  $\mathbf{s}_2(t)$  evolve with their mean distance being  $d^*$ .

The emergence of the nonzero stable fixed point  $d^*$  is strongly indicative of the chaotic nature of the transient dynamics in the ternary network. In particular, when  $d(t) = 0$  is the only stable fixed point in the Derrida plot in Fig. 1, a perturbation to a typical initial state, say,  $\mathbf{s}_1(0)$  and  $\mathbf{s}_2(0)$ , will lead to identical state evolutions of the ternary network:  $\mathbf{s}_1(t) = \mathbf{s}_2(t)$  for large  $t$ . Two distinct cases can arise. The first is when the two initial states evolve to the same fixed point attractor  $\mathbf{s}^*$ . The basin of this attractor can be large in the sense that, for any two states chosen from this basin as the initial states, their distance will go to zero as they both approach  $\mathbf{s}^*$ . An example of this case is shown in Fig. 2(a), where the upper panel displays the evolution of the normalized Hamming distance  $d(t)$  and the lower panel presents the evolution of the network states. The



**FIG. 1.** Representative mapping functions of the normalized Hamming distance  $d(t + 1)$  vs  $d(t)$  for a number of  $p$  values as determined by Eq. (3) for  $K = 2$ . The gray dashed diagonal line is  $d(t + 1) = d(t)$ .

initial distance is  $d(0) = 0.5$  in which half of the nodes have different initial values. This is not a small perturbation, but the distance decreases quickly to zero. This case is quite common. The second case is when the attractor is a periodic orbit in that both  $\mathbf{s}_1(t)$  and  $\mathbf{s}_2(t)$  fall on this orbit and evolve synchronously with  $\mathbf{s}_1(t) = \mathbf{s}_2(t)$ , as shown in Fig. 2(b). Note that here, the period is typically short. For example, when  $\mathbf{s}_1(0)$  and  $\mathbf{s}_2(0)$  yield the same  $\mathbf{s}_1(t) = \mathbf{s}_2(t)$  on a periodic orbit of period  $T$ , then  $\mathbf{s}_1(0)$  and  $\mathbf{s}_2(t_i)$  for  $t_i = 1, \dots, T - 1$  will lead to asynchronous evolution of  $\mathbf{s}_1(t)$  and  $\mathbf{s}_2(t)$  on the same orbit but with a nonzero distance  $d(t)$ . When  $T$  is small, the probability of synchronous evolution yielding  $d(t) = 0$  is high, but for large  $T$ , the asynchronous evolution dominates, yielding a nonzero distance  $d(t)$ . In fact, this is what happens about the transition point  $p_c = 2/3$ . Figure 2(c) shows an example with a nonzero  $d^*$ , e.g., the corresponding network state vectors  $\mathbf{s}_1$  and  $\mathbf{s}_2$  of length  $N$  fall onto the same periodic orbit of  $T = 21$  but with the lag of one time step, and their distance  $d(t)$  is not a constant but oscillates about  $d^*$ . It can also occur that  $\mathbf{s}_1$  and  $\mathbf{s}_2$  fall onto different attractors, with their mean normalized Hamming distance about  $d^*$ , as shown in Fig. 2(d). Note that in Figs. 2(c) and 2(d), short periodic orbits are chosen deliberately for visualization, whereas typical periods are much longer.

The key observation is that, for a finite distance  $d^*$ , in the  $N \rightarrow \infty$  limit, given an initial state  $\mathbf{s}(0)$ , a small initial perturbation  $d(0) \sim 0$  will grow exponentially, mimicking the exponential divergence of nearby orbits in chaotic systems. This leads to disordered dynamics of the ternary network. Note that “disordered” dynamics can be inferred from two facts in the  $N \rightarrow \infty$  limit: one is that the transient time is infinitely long and the other is that even in the steady state, the periods of most periodic orbits diverge. In a finite system, the transient behavior of an exponential increase in  $d(t)$  can

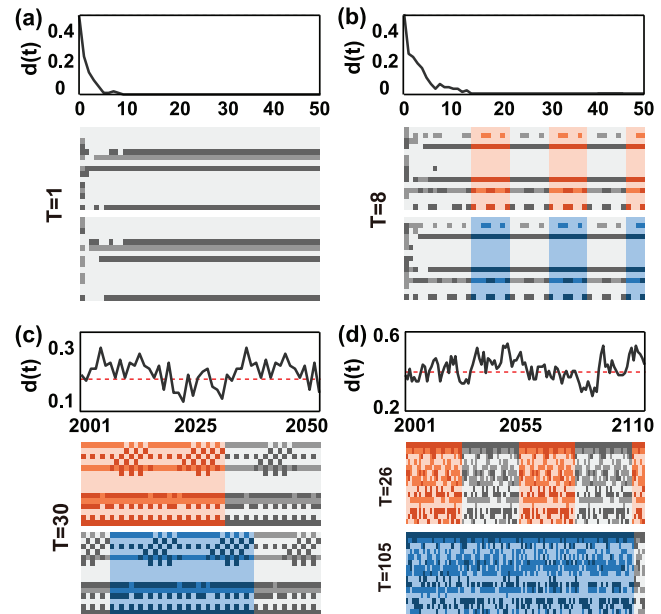


**FIG. 2.** Evolution of the normalized Hamming distance and the corresponding dynamical patterns of the steady periodic orbit structure. The ternary-network parameters are  $N = 100$  and  $K = 2$ . From (a) to (d), the parameters are  $p = 5/6, 3/4, 3/5, 1/2$  and  $d(0) = 0.5, 0.5, 0.1, 0.1$ , respectively. The values of the two state vectors  $\mathbf{s}_1(t)$  and  $\mathbf{s}_2(t)$  of 15 nodes (ordinate) are plotted in a time window of the same length as that in the corresponding upper panel, and the three state values are distinguished by the grayness. The colors in the lower panel of (b)–(d) mark the period  $T$  of the state evolution. Note that in (c) and (d), a transient time of 2000 steps has been disregarded, and short periodic orbits are chosen deliberately for visualization, although much longer periods are dominant.

be short, resulting in bounded oscillatory dynamics of the ternary network.

The possible occurrence of disordered dynamics in the ternary network for  $K = 2$  is surprising because this behavior is in sharp contrast to the Boolean logic dynamics where the system will remain in the ordered state with  $\lim_{t \rightarrow \infty} d(t) = 0$  for  $K = 2$ . (Recall that for the Boolean system, the condition under which a disordered state can arise is  $2p(1 - p)K > 1$ , but for  $K = 2$ , no possible value of  $0 \leq p \leq 1$  can be found to satisfy this inequality.) To further verify this, we specify pairs of random states  $\mathbf{s}_1$  and  $\mathbf{s}_2$  with fixed initial distance  $d(0) = 0.1$  and calculate their final distance vs  $p$  after evolving the ternary-network dynamics for time  $t$ , as shown in Fig. 3(a), where the network size is  $N = 500$ . The solid black curve is the solution  $d^*$  by setting  $d(t + 1) = d(t)$  in Eq. (3). The data points are the simulation results under three different simulation times  $t$ , and each point is an ensemble average of 500 runs. It can be seen that, as  $t$  increases, the agreement between the simulation and theoretical results becomes better. In fact, the data points at  $t = 100$  and  $t = 1000$  almost overlap on each other, indicating that  $t = 100$  is sufficient for the system to reach the final state. Figure 3(a) shows that the transition from disordered to ordered dynamics occurs at the predicted critical point  $p_c = 2/3$ , beyond which  $d^*$  becomes essentially zero. Figure 3(b) shows the average period  $\langle T \rangle$  laying

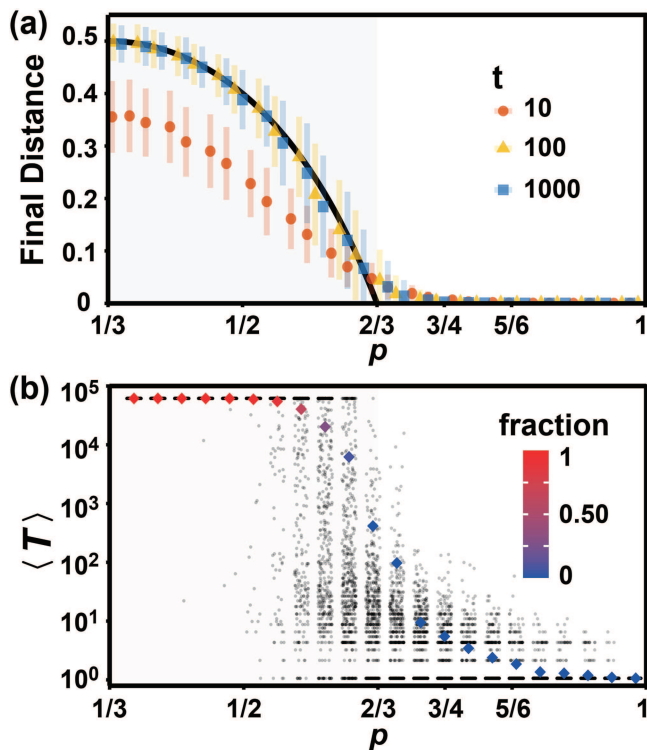


**FIG. 3.** (a) Asymptotic normalized Hamming distance vs  $p$ . The black solid curve is the nonzero solution  $d^*$  of  $d(t + 1) = d(t)$ . The initial distance is  $d(0) = 0.1$ . Three simulation times are used:  $t = 10, 100,$  and  $1000$ , as marked by circles, triangles, and squares, respectively. (b) Scattered plot of the period of the network state  $s(t)$  and the corresponding mean value. The scattered data points are broadened in the  $p$  direction for better visualization. A maximal value of  $T_{cut} = 50\,000$  is set, and if the period  $T$  is larger than  $T_{cut}$ , it is set to  $T_{cut}$ . The colors encode the fractions of the data points larger than  $T_{cut}$ . The gray shaded region specifies the  $p$  interval in which disordered dynamics arise. The network size is  $N = 500$ , and 500 random realizations are used for statistics.

over the scattered plot of the periods  $T$  of the ternary system in the steady state vs bias  $p$ . It is clear that in the ordered region  $p > 2/3$ ,  $\langle T \rangle$  is in the order of 1, which is mainly the fixed point attractor. Across the transition point  $p_c = 2/3$  to the disordered region,  $\langle T \rangle$  increases rapidly for several orders. Here, for networks of size  $N = 500$ , a  $T_{cut} = 50\,000$  is set. It can be seen that in the disordered region, a typical period of the periodic orbits is already larger than  $T_{cut}$ . As the period  $\langle T \rangle$  becomes so large, the dynamics is practically disordered.

To understand the emergence of disordered dynamics from a global point of view, we investigate the structure of the parameter plane  $(p, K)$ , or the phase diagram, for fixed network size  $N$ . Figure 4 depicts the parameter regions for disordered and ordered dynamics, where the solid black curve as determined by Eq. (4) specifies the boundary separating the two regions. To demonstrate that a characteristic change in the network dynamics will occur crossing the boundary, we fix  $K = 2$  and choose four values of  $p$  across the boundary: two on the left and two on the right of

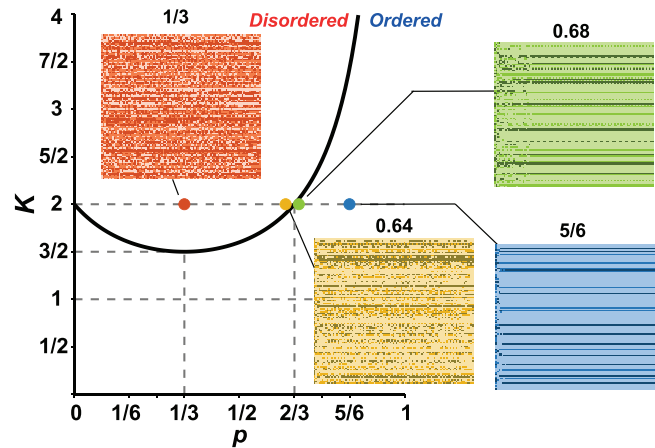


**FIG. 4.** Phase diagram in the parameter plane  $(p, K)$  and distinct spatiotemporal patterns of dynamical evolution. The critical curve in the parameter plane as determined by Eq. (4) separates a parameter plane into two distinct regions with ordered and disordered dynamics, respectively. The four illustrative patterns of spatiotemporal dynamical evolution in the insets are generated for  $N = 100$  and  $K = 2$ , where the value of the bias parameter  $p$  for each case is indicated at the top of the corresponding inset. In each inset, the horizontal and vertical axes denote time  $t$  in the range  $0 \leq t \leq 100$  and the index of the nodes in the ternary network in the range from 1 to  $N$ , respectively. The three possible values of the nodal dynamical state are distinguished by the depth of the color in each inset.

the boundary. The respective spatiotemporal patterns of dynamical evolution are shown in the insets, with the corresponding value of  $p$  specified at the top of each inset. In each case, the spatiotemporal evolution pattern starts from a random initial state, and the values of the ternary nodal states are distinguished by the color depth. For the two  $p$  values in the ordered region (the blue and green dots), the corresponding patterns become regular after an initial transient phase of disordered dynamics, where the transient is longer the closer the parameter value is to the boundary (the green dot and green evolution pattern). For the two  $p$  values to the left of the boundary (the yellow and red dots), the associated dynamical evolution patterns are persistently irregular. In principle, the nonlinear map [Eq. (3)] is valid only in the  $N \rightarrow \infty$  limit; therefore, for a finite system, the dynamical behavior near the boundary in the ordered region (e.g., the green dot) is not strictly the fixed point solution of Eq. (3), especially in a finite time. However, the overall behavior of transition between the ordered and disordered dynamics as predicted by Eqs. (3) and (4) agrees well with that calculated from the direct simulation of the ternary network.

Note that the boundary or the critical curve in the  $(p, K)$  plane reaches the minimal value in  $K$  ( $3/2$ ) for  $p = 1/3$ . As a result, for  $K < 3/2$ , disordered dynamics are ruled out. For large values of  $K$ , the critical transition point in  $p$  can be approximately determined by the relation  $p_c = [1 + \sqrt{4 - 6/K}]/3$ , where ordered and disordered dynamics arise for  $p > p_c$  and  $p < p_c$ , respectively. For  $K \gg 1$ , the value of  $p_c$  is close to one; therefore, disordered dynamics prevail for almost all values of  $p$ .

**B. Phase diagram and spatiotemporal dynamics for general biases**

We consider the general case with the bias set  $(p, q, r)$  with the normalization  $p + q + r = 1$ . To study the parameter space, it is convenient to use the triangular ternary representation, as shown in Fig. 5 and explained in its caption, where all allowed combinations of  $(p, q, r)$  are confined within the equilateral triangle. Specifically, for each point in the triangle, the values of  $(p, q, r)$  can be found from the cross points following the gray thick dashed lines to the boundary. We are able to derive a similar equation to Eq. (3) to describe the dynamical evolution of the normalized Hamming distance,

$$d(t + 1) = 2(1 - p^2 - q^2 - r^2 - pq - qr - rp)(1 - [1 - d(t)]^K). \tag{5}$$

The boundary separating the disordered and ordered regions in the triangular parameter space in Fig. 5 is determined by

$$p^2 + q^2 + r^2 + pq + qr + rp = 1 - \frac{1}{2K}, \tag{6}$$

which, for any given  $K$  value, generates a circle in the triangular ternary parameter space, as shown in Fig. 5 by a series of circular boundaries for different  $K$  values. For any circular boundary, the inner and outer regions are for disordered and ordered states, respectively. A larger value of  $K$  leads to a larger circle. The red circle for  $K = 2$  is exactly tangent to the triangular sides. Along each side of the triangle, one of the bias parameters is zero, e.g.,  $r = 0$  and  $p + q = 1$ ; therefore, it represents the degenerate case of the classical Boolean model. For example, with  $p + q = 1$ , Eq. (6) can be further simplified as  $p(1 - p) = 1/(2K)$ , which is exactly the formula determining the boundary between disordered and ordered dynamics in a classical Boolean network. Consequently, for  $K = 2$ , since the circle is tangent with the three sides, for the Boolean network, disordered states are ruled out, in accordance with our analysis in Sec. III A. The fractional values of  $K$  in Fig. 5 are the average numbers of inputs for a node in the network. For example,  $K = 3/2$ , half of the nodes in the network have one input, while the other half have two inputs. In this case, the circular boundary degenerates to a single point at the center of the triangle with parameter values  $(p, q, r) = (1/3, 1/3, 1/3)$ , indicating that no disordered states are possible. This corresponds to the minimum point of the boundary curve in Fig. 4, which is given by  $K = 3/2$  and  $p = q = 1/3$ .

**C. Lyapunov exponent of ternary networks**

In a classical Boolean network, the evolution of the distance between two infinitesimally close vectors, e.g., two  $N$ -bit Boolean trajectories  $\vec{x}(t)$  and  $\vec{y}(t)$ , can be conveniently characterized by the Lyapunov exponent.<sup>10</sup> In Boolean dynamics, the concept of a partial Boolean derivative<sup>31</sup> is essential,

$$\partial F_i / \partial x_j \equiv F_i(x_1, x_2, \dots, x_j, \dots) \oplus F_i(x_1, x_2, \dots, \neg x_j, \dots), \tag{7}$$

where  $\oplus$  and  $\neg$  represent Exclusive OR (XOR) and logical NOT operations, respectively. The value of the partial Boolean derivative evaluated at  $\vec{x}(t)$  is one if a change in the  $j$ th component  $x_j(t)$  causes a change in  $F_i$  or  $x_j(t + 1)$ ; otherwise, the derivative is zero. The Jacobin matrix  $\mathcal{J}(\vec{x}(t))$  is formed by all the partial Boolean derivatives, where  $(\partial F_i / \partial x_j)$  is the  $ij$ th element of the matrix. For two

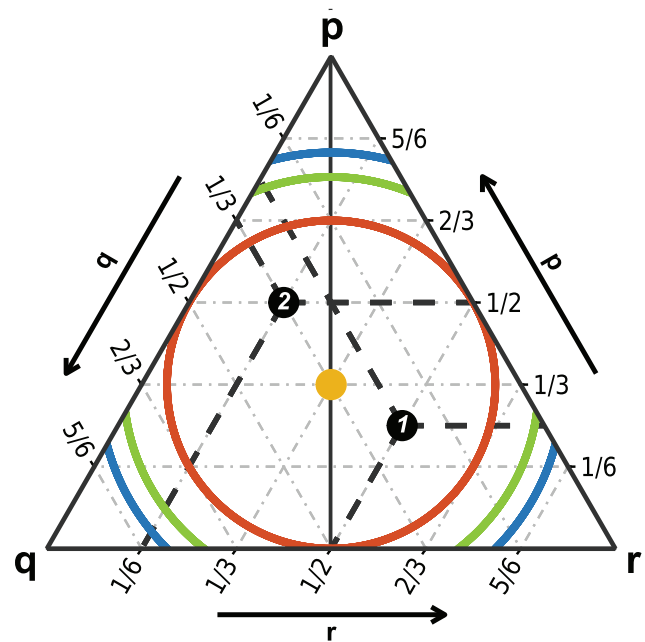


**FIG. 5.** Ternary phase diagram for general biases. Because of the constraint  $p + q + r = 1$ , the allowed values of these probabilities can be conveniently represented by the region inside the triangle, whose three sides correspond to  $p$ ,  $q$ , and  $r$ , respectively. Each point inside the triangle represents a unique bias set  $\{p, q, r\}$  for the three states  $\{\alpha, \beta, \gamma\}$ , whose values can be read out from the cross points following the gray thick dashed lines to the boundary, where each dashed line is parallel to a side of the triangle. For example, the black circles “1” and “2” correspond to the bias set  $\{1/4, 1/4, 1/2\}$  and  $\{1/2, 1/3, 1/6\}$ , respectively. The theoretical boundaries as determined by Eq. (6) separating the ordered and disordered regions for different  $K$  are indicated by the circles of different colors. From the circles inside out, the values of  $K$  are  $3/2, 2, 5/2$ , and  $3$ . For  $K = 3/2$ , the circle shrinks to a single point at the center of the triangle. The vertical line indicates the constrained case of  $(p, q, q)$ .

$N$ -bit Boolean vectors  $\vec{x}(t)$  and  $\vec{y}(t)$ , the difference in their bits can be described by  $\vec{\delta}(t) = \vec{x}(t) \oplus \vec{y}(t)$ , where  $\delta_i(t) = 1$  if  $x_i(t) \neq y_i(t)$  and zero otherwise. From the characteristics of XOR for Boolean variables, we have  $\vec{y}(t) = \vec{x}(t) \oplus \vec{\delta}(t)$ . The evolution of the difference/perturbation of two Boolean vectors  $\vec{x}(t)$  and  $\vec{y}(t)$  can then be described as<sup>10</sup>

$$\begin{aligned} \vec{\delta}(t + 1) &= \vec{x}(t + 1) \oplus \vec{y}(t + 1) \\ &= \mathbf{F}(\vec{x}(t)) \oplus \mathbf{F}(\vec{y}(t)) \\ &= \mathbf{F}(\vec{x}(t)) \oplus \mathbf{F}(\vec{x}(t) \oplus \vec{\delta}(t)). \end{aligned} \tag{8}$$

Making a linear approximation of the Boolean operations, we have<sup>32,33</sup>

$$\mathbf{F}(\vec{x}(t) \oplus \vec{\delta}(t)) \approx \mathbf{F}(\vec{x}(t)) \oplus \mathcal{J}(\vec{x}(t)) \odot \vec{\delta}(t),$$

which leads to

$$\vec{\delta}(t + 1) \approx \mathcal{J}(\vec{x}(t)) \odot \vec{\delta}(t),$$

where the operator  $\odot$  is defined as  $\text{sign}(\mathcal{J}(\vec{x}(t)) \cdot \vec{\delta}(t))$  with the sign function  $\text{sign}(0) = 0$  and  $\text{sign}(x > 0) = 1$ . Note that the sign function is used to normalize the output in the case where a bit is affected by two or more other bits. The probability of bits with two or more inputs goes to zero in the large  $N$  limit for fixed  $n$ , or when  $n/N \rightarrow 0$ , where

$$\vec{\delta}(t+1) \approx \mathcal{J}(\vec{x}(t)) \cdot \vec{\delta}(t).$$

The derivatives can be extended to our ternary system to define the Lyapunov exponent. In particular, a similar exclusive OR (XOR) operator  $\oplus_T$  can be defined to account for the differences between two vectors  $\vec{x}$  and  $\vec{y}$ ; i.e.,

$$\vec{\delta}(t) = \vec{x} \oplus_T \vec{y} = \mathbf{1} - \{\delta_{x_1,y_1}, \delta_{x_2,y_2}, \dots, \delta_{x_N,y_N}\}. \quad (9)$$

However, unlike the Boolean case, here, for a given  $\vec{x}$ , there can be different  $\vec{y}$ s yielding the same  $\vec{\delta}(t)$ . Nevertheless, the evolution of the difference  $\vec{\delta}(t)$  can be characterized in a similar way. Specifically, considering the large  $N$  limit and assuming initially that  $\vec{x}$  and  $\vec{y}$  only have a few bits that are different, we define a perturbation spread matrix  $\mathcal{D}$ , whose elements  $D_{ij}$  equal  $\tilde{p}$  if bit  $i$  has an input from bit  $j$ , where  $\tilde{p}$  is the probability that bit  $i$  is different at the next time step. We thus have

$$\vec{\delta}(t+1) = \langle \mathcal{D} \cdot \vec{\delta}(t) \rangle, \quad (10)$$

where  $\langle \cdot \rangle$  denotes the expectation value; i.e., if for one bit the value is  $\tilde{p}$ , then this bit is filled with one with the probability  $\tilde{p}$  and zero with probability  $1 - \tilde{p}$ . Defining the norm  $|\vec{\delta}(t)| = \sum_i \delta_i(t)$ , we have the Lyapunov exponent as<sup>10</sup>

$$\begin{aligned} \lambda &= \lim_{T \rightarrow \infty} 1/T \ln |\vec{\delta}_T| / |\vec{\delta}_0| \\ &= \ln \left\langle \frac{|\vec{\delta}(t+1)|}{|\vec{\delta}(t)|} \right\rangle = \ln \frac{|\langle \mathcal{D}(\vec{x}(t)) \cdot \vec{\delta}(t) \rangle|}{|\vec{\delta}(t)|}. \end{aligned} \quad (11)$$

Since the mapping functions are chosen randomly according only to the bias set  $(p, q, r)$ , when bit  $j$  is different, the probability for its successor, e.g., bit  $i$ , to take different values can be estimated as

$$\begin{aligned} \tilde{p} &= p(1-p) + q(1-q) + r(1-r) \\ &= 2(1-p^2 - q^2 - r^2 - pq - qr - rp), \end{aligned} \quad (12)$$

where the constraint  $p + q + r = 1$  has been used. As each node has  $K$  inputs chosen randomly from the other  $N - 1$  nodes, the average number of the outgoing connections for each node is also  $K$ . As a result, when there are  $n$  bits that are different between  $\vec{x}(t)$  and  $\vec{y}(t)$ , there will be on average  $nK\tilde{p}$  bits with one for  $\vec{\delta}(t+1)$  for  $N \gg n$ . These considerations lead to the following analytic expression for the Lyapunov exponent:

$$\lambda = \ln(K\tilde{p}) = \ln[2K(1-p^2 - q^2 - r^2 - pq - qr - rp)]. \quad (13)$$

The condition under which the ternary dynamics are unstable is thus

$$2K(1-p^2 - q^2 - r^2 - pq - qr - rp) > 1,$$

which is consistent with Eq. (6).

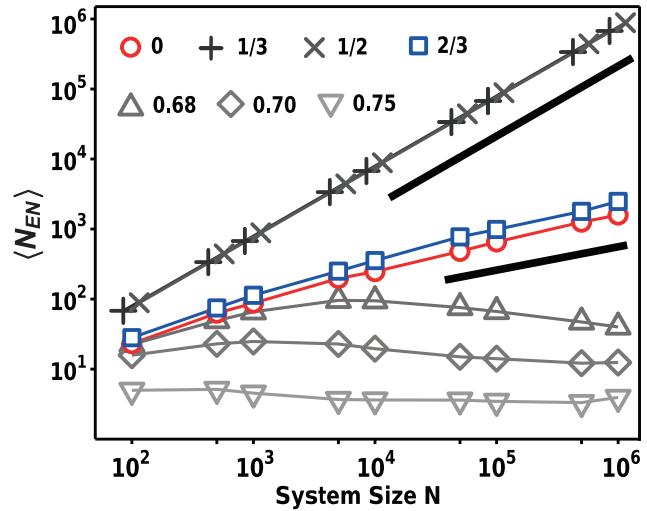


**FIG. 6.** Scaling laws governing the number of nodes engaged in the network dynamics. Shown is the average number  $\langle N_{EN} \rangle$  of engaged nodes vs the network size  $N$  for  $K = 2$  and different values of  $p$  in the constrained ternary model  $(p, q, r)$ . For  $0 < p < 2/3$ , the system is in a disordered state, leading to the scaling relation  $\langle N_{EN} \rangle \sim N$ . For  $p > 2/3$ , the system is in an ordered state and  $\langle N_{EN} \rangle$  approaches a constant value. At the critical point  $p = 2/3$ , the scaling law is  $\langle N_{EN} \rangle \sim N^{1/3}$  for large  $N$ . The two thick line segments indicate the scaling exponents of 1 and 1/3, respectively. Each data point is the result of averaging over 1000 independent dynamical realizations.

#### D. Number of nodes engaged in dynamics: Scaling laws

A useful concept to identify disordered dynamics in discrete logic systems is the “engaged nodes,” which are those that are involved or engaged in determining the final state of the system.<sup>9,11,12</sup> These nodes can be identified as follows. One first identifies the “fixed” or “frozen” nodes whose outputs are entirely independent of their inputs. The nodes whose outputs depend only on the inputs from other frozen nodes will also be frozen nodes, which can be identified using an iterative procedure. Note that there can be higher order effects, leading to the frozen nodes due to the correlation between the inputs from different engaged nodes.<sup>11</sup> The frozen nodes and other nodes with no relevant outputs are removed, and the remaining nodes are those engaged in the system dynamics, whose number is denoted as  $N_{EN}$ .

If  $N_{EN}$  is a constant or increase slowly with the system size, the system is scalable in the sense of controllability.<sup>12</sup> We first consider a constrained ternary network where there is only one bias parameter  $p$  ( $q = (1 - p)/2$ ) for  $K = 2$ . Figure 6 shows the average number of the engaged nodes vs the network size. It can be seen that, in the disordered region  $p < 2/3$ , the number of the engaged nodes is comparable and proportional to the system size. However, at the critical point of  $p_c = 2/3$  or  $p_c = 0$ , we have  $\langle N_{EN} \rangle \sim N^{1/3}$  in the large  $N$  limit (see Appendix C for details). In the ordered region  $p > 2/3$ ,  $\langle N_{EN} \rangle$  is approximately a constant, regardless of the network size. There is, therefore, a characteristic change in the scaling of  $\langle N_{EN} \rangle$  with the system size upon a transition between ordered

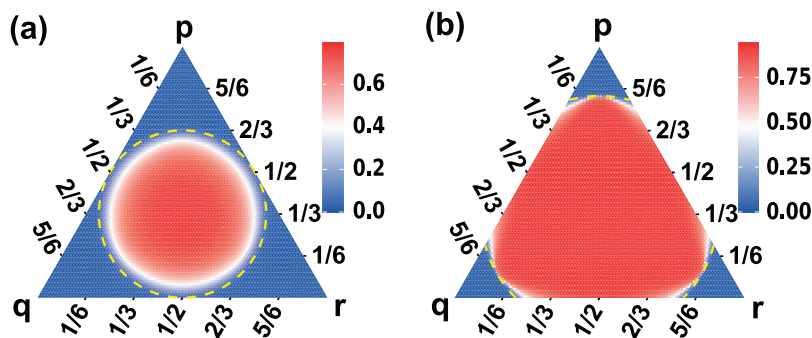


FIG. 7. Fraction  $(N_{EN})/N$  of engaged nodes in the ternary network for  $K = 2$  (a) and  $K = 3$  (b) in the  $(p, q, r)$  parameter space. The dashed curves indicate the domain boundary from Eq. (6). System size  $N$  is fixed at 10 000. Each point in the diagram is the result of averaging 1000 realizations for reliable statistics.

and disordered dynamics. Thus, for our ternary network, the system is scalable only in the ordered state; e.g.,  $p > 2/3$  for  $K = 2$ . This should be contrasted to the classical Boolean network where for  $K = 2$ , the disordered parameter region shrinks to a single point and therefore, the network always scalable.<sup>12</sup>

If the fraction of the engaged nodes is large, the dynamics are more likely to be disordered. For each point in the ternary parameter space (a given combination of  $\{p, q, r\}$ ) in Fig. 5, we carry out an ensemble of 1000 simulations. In each run, the engaged nodes are identified, and the average fraction of these nodes is calculated. The results for  $K = 2$  and  $K = 3$  are shown in Figs. 7(a) and 7(b), respectively. In each case, a sharp circular boundary emerges in the ternary parameter space, separating the whole parameter space into disordered and ordered regions, which is consistent with the results in Fig. 6.

#### IV. DISCUSSION

Boolean networks are a paradigm not only in biology for gaining quantitative insights into systems, such as gene regulatory networks, but also in other fields for understanding a variety of complex dynamical behaviors. A Boolean network of size  $N$  is a deterministic and self-evolving dynamical system with  $N$  binary state variables that can be represented by an  $N$ -bit binary vector, where the total number of possible states is  $2^N$ . Starting from a random initial condition, the system typically evolves into a final state that can be a fixed point attractor or a periodic attractor. In many biological contexts, e.g., gene regulatory networks, such a description is natural and adequate. While the paradigm of Boolean networks has enjoyed remarkable success in characterizing and understanding a variety of phenomena, there are situations in biology where a binary Boolean description is fundamentally inadequate. For example, to understand the gene product concentration gradient effect requires distinct response thresholds,<sup>34–36</sup> a situation that cannot be accommodated by a binary network model. Biosystems can have multiple stable states with distinct concentration levels, which correspond to multi cell fates<sup>37–39</sup> or system marks, such as p53-induced oscillations<sup>40–42</sup> or EMT processes.<sup>43–46</sup> For these systems, a description beyond the Boolean paradigm is needed.

We have articulated a random ternary-network model as a generalization of classical Kauffman Boolean networks and analyzed its dynamical behaviors. In a random ternary network of  $N$  nodes,

each node has  $K$  inputs chosen randomly from the other  $N - 1$  nodes. However, the state of each node can now be in one of the three states, and there are in total  $3^{3^K}$  possible mapping functions. The outputs of these mapping functions have equal probabilities to take on the three discrete values. To enable parameter variations as in realistic biological situations, a set of bias parameters is necessary, which specify the probabilities of the three states appearing in the system output. In model implementation, this is equivalent to choosing the mapping functions that yield different outputs with the specific bias probabilities. Due to the random and probabilistic nature of the underlying system, its dynamics should be analyzed through the mean field approach with measures, such as the Derrida plot<sup>7</sup>—a kind of return map in nonlinear dynamics, which captures the evolution of the distance between two states in a geometrically intuitive way. The geometric approach makes it convenient to analyze the conditions under which the system will evolve into an ordered or a disordered state and to determine the stability of the final state. The approach also allows a Hamming-distance based Lyapunov exponent to be defined and calculated for large systems, where a positive (negative) exponent signifies a disordered (ordered) state. We have also studied the engaged nodes,<sup>9,11,12</sup> and their role in determining the dynamical scalability of the systems with the finding that a ternary network is generally scalable in the ordered phase but unscalable in the disordered phase. In particular, when the final state is disordered, the number of nodes engaged in the dynamical process grows algebraically with the system size. At the critical point where a ternary network effectively reduces to the classical Boolean network, the scaling behaviors also agree with each other exactly. In addition, the boundary separating the scalable and unscalable phase in the parameter space coincides with the boundary between the ordered and disordered states, as they both correspond to the critical point determined by the mean field theory.

Our ternary networks provide a framework that enables much richer dynamical behaviors than allowed by the classical Boolean networks. From the point of view of nonlinear dynamics, the ternary networks represent a new “playground” to explore, understand, and exploit a rich variety of behaviors. For example, to identify natural phenomena that defy the classical Boolean description but can be faithfully modeled by ternary-network dynamics is an urgent topic warranting further efforts. To devise a self-consistent scheme to enable logic operations in ternary networks is another problem worth investigating with potential applications in computing.

## ACKNOWLEDGMENTS

This work was supported by the National Key R&D Program of China under Grant No. 2019YFA0110200; by the NSFC under Grant Nos. 12175090, 11775101, 12047501, 31830060, and 92068201; by the 111 Project under Grant No. B20063; and by the CAS Key Laboratory of Regenerative Biology, Guangdong Provincial Key Laboratory of Stem Cell and Regenerative Medicine, Guangzhou Institutes of Biomedicine and Health, Chinese Academy of Sciences. The work at Arizona State University was supported by the Office of Naval Research through Grant No. N00014-21-1-2323.

## AUTHOR DECLARATIONS

### Conflict of Interest

The authors have no conflicts to disclose.

## DATA AVAILABILITY

The data that support the findings of this study are available from the corresponding author upon reasonable request.

## APPENDIX A: SIMULATION DETAILS

### 1. Random ternary network

The network has  $N$  nodes, and each node has  $K$  input links that are chosen randomly from the other  $N - 1$  nodes. As a node has  $K$  input variables and each variable can take on three possible values, there are in total  $3^K$  possible input vectors. For each node  $i$ , its output is determined from the  $K$  inputs by

$$s_i(t+1) = f_i(s_{i_1}(t), s_{i_2}(t), \dots, s_{i_K}(t)), \quad (\text{A1})$$

where  $f_i(\cdot)$  is the mapping function that is typically represented by a discrete mapping table with  $3^K$  rows. Each of the  $3^K$  possible input vectors is mapped to a specific value of  $\alpha$ ,  $\beta$ , or  $\gamma$ . There are in total  $3^{3^K}$  possible mapping functions. For the random  $N$ - $K$  ternary network with the bias set  $(p, q, r)$ , a feasible procedure to determine all the  $N$  mapping functions is to first list all the possible  $3^{KN}$  input vectors sequentially for all the nodes and then fill the  $3^{KN}$  rows of the mapping table with  $\alpha$ ,  $\beta$ , and  $\gamma$  according to the specific probabilities  $p$ ,  $q$ , and  $r$ , respectively, where  $p + q + r = 1$ .

The ternary system is, in fact, deterministic because once the mapping functions are chosen, they are fixed. For a given initial state, the nodes update their values in a parallel manner following their respective mapping functions (synchronous updating rules).

### 2. Dynamical evolution of the Hamming distance

To calculate the dynamical evolution of the normalized Hamming distance, we first set one random ternary vector  $\mathbf{s}_1$  of length  $N$  as the initial state. We then choose  $d(0) \cdot N$  nodes randomly and, for each node, replace its value by the other two different values with equal probability, e.g.,  $\alpha \rightarrow \beta$  or  $\gamma$ , generating another initial state  $\mathbf{s}_2$ . From both states, the random ternary network evolves following the same mapping function set. Specifically, for each node  $i$ , with the  $K$  inputs, its output is uniquely determined by Eq. (A1). All the nodes update their states (outputs) simultaneously. At each

time step, the normalized Hamming distance between the two states is given by Eq. (2).

### 3. Identification of frozen nodes and engaged nodes

For a given random ternary network, we first examine the mapping functions and identify the nodes with constant outputs regardless of their inputs. For these nodes, the mapping tables always yield a constant value, e.g., either  $\alpha$ ,  $\beta$ , or  $\gamma$  for all possible inputs. This case will become more prevalent when the system is more biased, e.g., closer to the corners in the ternary  $(p, q, r)$  parameter space. These are the frozen nodes as their outputs never change. For the remaining nodes, those whose inputs are all from the frozen nodes are also identified as frozen nodes as their inputs are constant so that their outputs will be frozen, too. This procedure is carried out recursively until no new frozen nodes can be found. The remaining nodes have changing state variables, but they are not always engaged nodes. There are two cases where the outputs of those nodes do not lead to changes of the states of the other nodes: (1) the node has zero out-links and (2) the out-links are all connected to frozen nodes. Except for these two cases, all the remaining nodes are identified as the engaged nodes as they are involved in determining the final state of the system.

## APPENDIX B: DERIVATION OF EQ. (3)

Equation (3) is for the case of the special bias set:  $\{p, q, q\} = \{p, (1-p)/2, (1-p)/2\}$  with  $0 < p < 1$  being the control parameter. Following Derrida's work,<sup>7</sup> we employ the normal Hamming distance and the annealed approximation to quantify the system's degree of order. The three states  $\{\alpha, \beta, \gamma\}$  are on an equal footing, and the distance between two ternary-type vectors measures the number of differing bits. Let  $n$  be the initial number of differing bits between the two vectors (so that they possess  $N - n$  identical bits). We aim to calculate an asymptotic distance as a result of the dynamical iteration of the ternary  $N$ - $K$  model.

One node is a stable inheritance if its inputs are all from the set of the  $N - n$  identical bits, and this node will take the same value in the next step. Let  $N_0$  be the number of such inheritance nodes, and the corresponding probability is

$$P_{N_0} = C_N^{N_0} [(1 - n/N)^K]^{N_0} [1 - (1 - n/N)^K]^{N - N_0}, \quad (\text{B1})$$

where  $1 - n/N$  is the probability of choosing one node as an input and the inputs are the same for the two initial vectors and  $(1 - n/N)^K$  is the probability that all the  $K$  inputs for a node are the same. For all the  $N_0$  bits, each has the same inputs for the two vectors, and they will be the same at the next step.

The  $N - N_0$  remaining bits have different inputs. Nevertheless, the mapping function may still return the same output, e.g., with probability  $p_s$ , and  $p_u = 1 - p_s$  is the probability to have a different output. The number  $m$  of the bits with different values follows the distribution,

$$P_{n \rightarrow m} = \sum_{N_0=0}^{N-m} P_{N_0} \cdot C_{N-N_0}^m p_u^m p_s^{N-N_0-m}, \quad (\text{B2})$$

where the summation is over all possible  $N_0$ s yielding the same  $m$ . Substituting Eq. (B1) for  $P_{N_0}$  into the above equation, we have

$$P_{n \rightarrow m} = \frac{N!}{m!(N-m)!} p_u^m \left[ 1 - \left( 1 - \frac{n}{N} \right)^K \right]^m \times \left\{ \left( 1 - \frac{n}{N} \right)^K + p_s \left[ 1 - \left( 1 - \frac{n}{N} \right)^K \right] \right\}^{N-m}. \quad (B3)$$

Equation (B3) is the general form of the probability  $P_{n \rightarrow m}$ . In a Boolean system, the following relations hold:<sup>7-9</sup>  $p_s = p^2 + (1-p)^2$  and  $p_u = 2p(1-p)$ . In our ternary system, the biases ( $p, q, r$ ) are the respective probabilities for the three states  $\alpha, \beta$ , and  $\gamma$  to arise. When the inputs are different, the output is determined uniquely by probabilities ( $p, q, r$ ) and is independent of its previous state, even with a fixed mapping function for this bit. As a result, the probabilities that the two bits are the same and different are  $p_s = p^2 + 2q^2$  and  $p_u = p(1-p) + 2q(1-q) = (1-p)(3p+1)/2$ , respectively. The final form of the transition probability from the  $n$  differing bits at the previous step to  $m$  distinct bits at the current step is given by

$$P_{n \rightarrow m} = \frac{N!}{m!(N-m)!} \left[ \frac{(1-p)(3p+1)}{2} \right]^m \left[ 1 - \left( 1 - \frac{n}{N} \right)^K \right]^m \times \left\{ \left( 1 - \frac{n}{N} \right)^K + \left[ 1 - \frac{(1-p)(3p+1)}{2} \right] \right\} \times \left[ 1 - \left( 1 - \frac{n}{N} \right)^K \right]^{N-m}. \quad (B4)$$

For large  $N$  but  $n \ll N$  and  $m \ll N$ , we define  $x = n/N$  and  $y = \langle m \rangle / N$  to obtain

$$y = (1-p)(3p+1)/2 \cdot [1 - (1-x)^K]. \quad (B5)$$

Noting that  $x$  is actually  $d(t)$  and  $y$  is  $d(t+1)$ , we have

$$d(t+1) = (1-p)(3p+1)/2 \cdot [1 - (1-d(t))^K], \quad (B6)$$

which is Eq. (3) in the main text.

An assumption employed in the above derivation is that the updating rules are completely random and are determined solely by the bias set.<sup>7</sup> This annealed approximation ignores the correlation between the dynamical variables at different iterations, which effectively treats the ternary dynamics as a Markovian process.

### APPENDIX C: STABLE CORE AND SCALING LAW OF THE NUMBER OF ENGAGED NODES AT THE CRITICAL POINT

We adopt the concept of frozen core and derive the scaling law for the engaged nodes at the critical point of the ternary network. In particular, the frozen core is the set of nodes with time-invariant outputs,<sup>9</sup> which are stable nodes. Let  $s(t)$  be the fraction of the nodes in the frozen core relative to the system size  $N$ . Initially,  $s(0)$  is then the probability of choosing constant mapping functions whose output does not depend on the inputs after an initial configuration. The

time evolution of  $s(t)$  is given by

$$s(t+1) = \sum_{k=0}^K C_K^k s(t)^{K-k} (1-s(t))^k p_k \equiv f(s(t)), \quad (C1)$$

where  $K$  is the number of inputs of each node and  $p_k$  is the probability when a node has  $K-k$  inputs from the frozen core and its output is independent of the  $k$  other inputs. In this case, this node is solely determined by the frozen core and will be part of it thereafter, leading to  $p_0 = 1$ . Once the series  $\{p_k, k = 0, \dots, K\}$  is obtained for a given  $K$  value, the evolution of  $s(t)$  is determined.

Note that  $s_\infty = f(s_\infty)$  gives the fixed points of the fraction of the frozen core, and  $s = 1$  is the trivial solution that the whole system becomes frozen. A Derrida curve representing the iterative relation  $s(t+1) = f(s(t))$  is a non-decreasing function because of the growth of  $s(t)$  with time. Especially, for any  $K$ , we have  $f'(1) = K(1-p_1)$ . For  $f'(1) > 1$ , the fixed point  $s = 1$  loses its stability, while another stable point  $s_\infty$  emerges; therefore,  $f'(1) = K(1-p_1) = 1$  gives the critical condition that the whole system belongs to the frozen core.<sup>9</sup> However, the  $k$  inputs are not necessarily independent; therefore, the condition  $K(1-p_1) = 1$  is appropriate only for the case of  $N \rightarrow \infty$ .

For ternary networks, it suffices to focus on the quantity  $p_1$ . Recall that the number of possible mapping functions is  $3^{3^K}$ . For the  $k$  inputs that are not from the frozen core, there are two cases. The first is that the input and, therefore, the output of the other nodes can be any of the  $\{\alpha, \beta, \gamma\}$  values, signifying a totally uncertain case. The second case is that the output can take on two values, e.g.,  $\{\alpha, \beta\}$ , giving rise to a partially uncertain case. Note that if the output of a node can take on only one value, the node will belong to the frozen core. The quantity  $p_1$  can then be expressed as

$$p_1 = w \cdot (p^3 + q^3 + r^3) + u \cdot (p^2 + q^2 + r^2),$$

where  $w$  and  $u$  are the respective fractions of the totally and partially uncertain nodes in the network. To simplify the expression, we set

$$\tilde{p}_{k,(1)} = \sum_{0 < n_u, n_w}^{n_u + n_w = k} f(n_u, n_w) p_{n_u, n_w}^{(1)}$$

as the probability of  $k$  unstable inputs leaving a constant output, where  $f(n_u, n_w)$  is the number of possibilities of exactly  $n_u$  partially and  $n_w$  totally uncertain signals with the corresponding probability  $p_{n_u, n_w}^{(1)}$ . The superscript (1) means that the output is a constant, and superscripts (2) and (3) are for the cases of partial and total uncertainty, respectively.

To obtain the relative fractions of  $u$  and  $w$ , it is necessary to analyze the feature of the remaining network outside the frozen core, which is composed of unstable nodes. For  $K = 2$ , after identification of the stable frozen core nodes, the average in-degree of the unstable nodes is between one and two,

$$\langle k_{in} \rangle = \frac{C_2^1(N-U-W)(U+W)\tilde{q}_{1,(1)} + 2(U+W)^2\tilde{q}_{2,(1)}}{C_2^1(N-U-W)(U+W)\tilde{q}_{1,(1)} + (U+W)^2\tilde{q}_{2,(1)}} \simeq 1 + \frac{\tilde{q}_{2,(1)}}{2\tilde{q}_{1,(1)}} \frac{U+W}{N} + \left( \frac{\tilde{q}_{2,(1)}}{2\tilde{q}_{1,(1)}} - \frac{\tilde{q}_{2,(1)}^2}{4\tilde{q}_{1,(1)}^2} \right) \frac{(U+W)^2}{N^2},$$

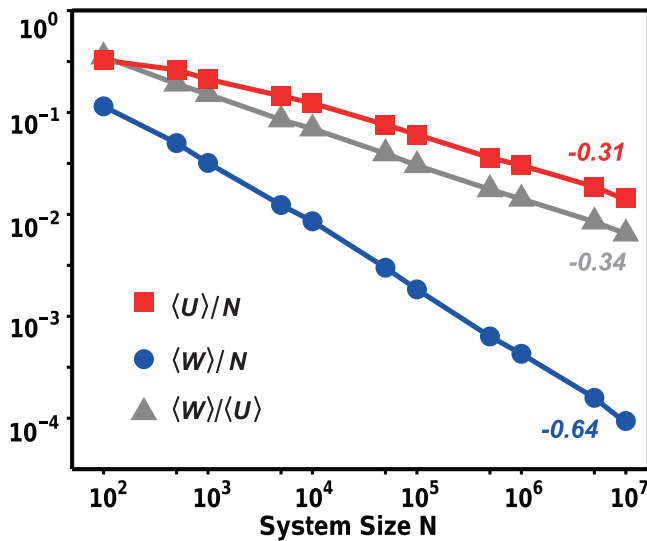


**FIG. 8.** Scaling relations at the critical point. Shown are  $\langle U \rangle$ ,  $\langle W \rangle$ , and  $\langle W \rangle/\langle U \rangle$  vs the system size  $N$  for  $K = 2$  at critical point  $p = 2/3$ , represented by the red squares, the gray triangles, and the blue circles, respectively. Each data point is the result of averaging over  $\max(1000, 0.01N)$  realizations.

where  $\tilde{q}_{k,(1)} = 1 - \tilde{p}_{k,(1)}$  and  $U$  and  $W$  stand for the numbers of partially and totally uncertain nodes ( $U = uN$  and  $W = wN$ ), respectively. In the ordered regime and at the criticality, the number of unstable nodes is much smaller than the system size.<sup>12</sup> In the limit  $N \rightarrow \infty$ , both  $U/N$  and  $W/N$  go to zero, as illustrated in Fig. 8. We, therefore, have  $\langle k_{in} \rangle \rightarrow 1$ . Furthermore, the zero out-degree nodes are removed; therefore, most of the engaged nodes form many loops with single inputs. Defining  $u' = u/(u + w)$  and  $w' = w/(u + w)$ , we obtain the update functions of  $u'$  and  $w'$  as

$$\begin{cases} u'(t+1) \simeq u'(t) + p_{0,1}^{(2)}/(p_{0,1}^{(2)} + p_{0,1}^{(3)}) \cdot w'(t), \\ w'(t+1) \simeq p_{0,1}^{(3)}/(p_{0,1}^{(2)} + p_{0,1}^{(3)}) \cdot w'(t). \end{cases} \quad (C2)$$

Since both  $p_{0,1}^{(3)}$  and  $p_{0,1}^{(2)}$  for the total and partial uncertainty are positive, we have  $w' \rightarrow 0$  and  $u' \rightarrow 1$ . Consequently, the partially uncertain nodes occupy most of the components of the engaged nodes. We have

$$\tilde{p}_{1,(1)} = f(1, 0)p_{1,0}^{(1)} + f(0, 1)p_{0,1}^{(1)} \approx p_{1,0}^{(1)},$$

where  $p_{1,0}^{(1)}$  is the probability that the output is a constant when there is only one input with partial uncertainty,

$$p_{1,0}^{(1)} = p^2 + q^2 + r^2.$$

Assuming  $q = r = (1 - p)/2$ , we obtain the critical condition from  $K(1 - \tilde{p}_{1,(1)}) = 1$  as  $2p - 3p^2 = 0$  or  $p_c = 2/3$  and zero, where the former is for the ternary network while the latter  $p_c = 0$  and consequently  $q = r = 0.5$  degenerates into the Boolean case. The remaining system of unstable or engaged nodes is analogous to the critical Boolean network,<sup>12,47</sup> for which the relative component size scales with the system size as  $\langle N_{EN} \rangle \sim N^{1/3}$ .

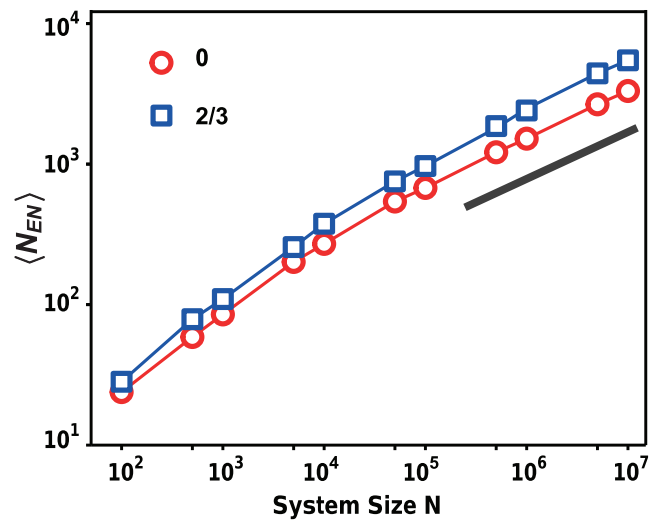


**FIG. 9.** Scaling of the size of the network component engaged in ternary dynamics. Shown is  $\langle N_{EN} \rangle$  vs  $N$  for  $K = 2$  at the critical points  $p = 2/3$  and  $p = 0$  for the bias set is  $(p, q, q)$ . The short line segment has a slope of  $1/3$ . Each data point is the result of averaging over  $\max(1000, 0.01N)$  simulation realizations.

Alternatively, at the critical point, the network component of engaged nodes can be viewed as a maximum percolation cluster. It is equivalent to constructing a random network that each newly added unstable node outputs an uncertain signal. In the limit  $N \rightarrow \infty$ , the condition under which the component of engaged nodes grows is that the average uncertain output of a node receiving uncertain inputs is one, i.e.,  $K(1 - p_1) = 1$ , which is exactly the critical condition. Figure 9 shows the average size of the component of engaged nodes  $\langle N_{EN} \rangle$  vs the system size  $N$  at the critical points  $p_c = 0$  and  $2/3$ . Note that the curve for  $p_c = 2/3$  is slightly higher than the one for  $p_c = 0$ , which can be attributed to the complexity of the multi-valued dynamical process. Nevertheless, the scaling exponents for large  $N$  for the two critical points are the same.

REFERENCES

- <sup>1</sup>S. A. Kauffman, "Homeostasis and differentiation in random genetic control networks," *Nature* **224**, 177–178 (1969).
- <sup>2</sup>S. A. Kauffman, "Metabolic stability and epigenesis in randomly constructed genetic nets," *J. Theor. Biol.* **22**, 437–467 (1969).
- <sup>3</sup>D. Stauffer, "Percolation thresholds in square-lattice Kauffman model," *J. Theor. Biol.* **135**, 255–261 (1988).
- <sup>4</sup>M. D. Stern, "Emergence of homeostasis and "noise imprinting" in an evolution model," *Proc. Natl. Acad. Sci. U.S.A.* **96**, 10746–10751 (1999).
- <sup>5</sup>M. Paczuski, K. E. Bassler, and A. Corral, "Self-organized networks of competing Boolean agents," *Phys. Rev. Lett.* **84**, 3185–3188 (2000).
- <sup>6</sup>S. Kochemazov and A. Semenov, "Using synchronous Boolean networks to model several phenomena of collective behavior," *PLoS One* **9**, e115156 (2014).
- <sup>7</sup>B. Derrida and Y. Pomeau, "Random networks of automata: A simple annealed approximation," *Europhys. Lett.* **1**, 45–49 (1986).
- <sup>8</sup>B. Derrida and H. Flyvbjerg, "Multivalley structure in Kauffman's model: Analogy with spin glasses," *J. Phys. A: Math. Gen.* **19**, L1003–L1008 (1986).
- <sup>9</sup>H. Flyvbjerg, "An order parameter for networks of automata," *J. Phys. A: Math. Gen.* **21**, L955–L960 (1988).

- <sup>10</sup>B. Luque and R. V. Sole, "Lyapunov exponents in random Boolean networks," *Physica A* **284**, 33–45 (2000).
- <sup>11</sup>S. Bilke and F. Sjunnesson, "Stability of the Kauffman model," *Phys. Rev. E* **65**, 016129 (2001).
- <sup>12</sup>J. E. S. Socolar and S. A. Kauffman, "Scaling in ordered and critical random Boolean networks," *Phys. Rev. Lett.* **90**, 068702 (2003).
- <sup>13</sup>B. Drossel, T. Mihajev, and F. Greil, "Number and length of attractors in a critical Kauffman model with connectivity one," *Phys. Rev. Lett.* **94**, 088701 (2005).
- <sup>14</sup>S. Squires, A. Pomerance, M. Girvan, and E. Ott, "Stability of Boolean networks: The joint effects of topology and update rules," *Phys. Rev. E* **90**, 022814 (2014).
- <sup>15</sup>R. Thomas, "Regulatory networks seen as asynchronous automata: A logical description," *J. Theor. Biol.* **153**, 1–23 (1991).
- <sup>16</sup>I. Shmulevich, E. R. Dougherty, S. Kim, and W. Zhang, "Probabilistic Boolean networks: A rule-based uncertainty model for gene regulatory networks," *Bioinformatics* **18**, 261–274 (2002).
- <sup>17</sup>F. Li, T. Long, Y. Lu, Q. Ouyang, and C. Tang, "The yeast cell-cycle network is robustly designed," *Proc. Natl. Acad. Sci. U.S.A.* **101**, 4781–4786 (2004).
- <sup>18</sup>R. Schlatter, K. Schmich, I. Avalos Vizcarra, P. Scheurich, T. Sauter, C. Borner, M. Ederer, I. Merfort, and O. Sawodny, "On/off and beyond—A Boolean model of apoptosis," *PLoS Comput. Biol.* **5**, e1000595 (2009).
- <sup>19</sup>K. Mangla, D. L. Dill, and M. A. Horowitz, "Timing robustness in the budding and fission yeast cell cycles," *PLoS One* **5**, e8906 (2010).
- <sup>20</sup>C. Hong, M. Lee, D. Kim, D. Kim, K. Cho, and I. Shin, "A checkpoints capturing timing-robust Boolean model of the budding yeast cell cycle regulatory network," *BMC Syst. Biol.* **6**, 129 (2012).
- <sup>21</sup>F. Gómez, I. Khoury, J. Kienzle, E. Mcleish, and A. Melvin, "Mathematical models for binarization and ternarization of musical rhythms," in *BRIDGES: Mathematical Connections in Art, Music and Science*, edited by R. Sarhangi and J. Barrallo [Tarquin Publications, San Sebastian (Donostia), Spain, 2007], pp. 99–108.
- <sup>22</sup>F. Li, B. Zhang, and B. Liu, "Ternary weight networks," [arXiv:1605.04711](https://arxiv.org/abs/1605.04711) (2016).
- <sup>23</sup>C. Zhu, S. Han, H. Mao, and W. J. Dally, "Trained ternary quantization," in *5th International Conference on Learning Representations, ICLR 2017* (OpenReview.net, Toulon, France, 2017).
- <sup>24</sup>C. Leng, Z. Dou, H. Li, S. Zhu, and R. Jin, "Extremely low bit neural network: Squeeze the last bit out with ADMM," in *The Thirty-Second AAAI Conference on Artificial Intelligence* (AAAI Press, New Orleans, LA, 2018), Vol. 32, pp. 3466–3473.
- <sup>25</sup>Y. Xu, Y. Wang, A. Zhou, W. Lin, and H. Xiong, "Deep neural network compression with single and multiple level quantization," in *The Thirty-Second AAAI Conference on Artificial Intelligence* (AAAI Press, New Orleans, LA, 2018), Vol. 32, pp. 4335–4342.
- <sup>26</sup>Z. He and D. Fan, "Simultaneously optimizing weight and quantizer of ternary neural network using truncated Gaussian approximation," in *2019 IEEE/CVF Conference on Computer Vision and Pattern Recognition, CVPR 2019* (IEEE Computer Society, Long Beach, CA, 2019), pp. 11430–11438.
- <sup>27</sup>A. Marban, D. Becking, S. Wiedemann, and W. Samek, "Learning sparse & ternary neural networks with entropy-constrained trained ternarization (EC2T)," in *2020 IEEE/CVF Conference on Computer Vision and Pattern Recognition Workshops (CVPRW)* (IEEE, Seattle, WA, 2020), pp. 3105–3113.
- <sup>28</sup>B. Derrida and D. Stauffer, "Phase transitions in two-dimensional Kauffman cellular automata," *Europhys. Lett.* **2**, 739–745 (1986).
- <sup>29</sup>S. A. Kauffman, "Requirements for evolvability in complex systems: Orderly dynamics and frozen components," *Physica D* **42**, 135–152 (1990).
- <sup>30</sup>I. Shmulevich and S. A. Kauffman, "Activities and sensitivities in Boolean network models," *Phys. Rev. Lett.* **93**, 048701 (2004).
- <sup>31</sup>G. Y. Vichniac, "Boolean derivatives on cellular automata," *Physica D* **45**, 63–74 (1990).
- <sup>32</sup>F. Bagnoli, "Boolean derivatives and computation of cellular automata," *Int. J. Mod. Phys. C* **03**, 307–320 (1992).
- <sup>33</sup>F. Bagnoli and R. Rechtman, "Synchronization and maximum Lyapunov exponents of cellular automata," *Phys. Rev. E* **59**, R1307–R1310 (1999).
- <sup>34</sup>H. L. Ashe and J. Briscoe, "The interpretation of morphogen gradients," *Development* **133**, 385–394 (2006).
- <sup>35</sup>K. W. Rogers and A. F. Schier, "Morphogen gradients: From generation to interpretation," *Annu. Rev. Cell Dev. Biol.* **27**, 377–407 (2011).
- <sup>36</sup>C. Carmona-Fontaine, M. Deforet, L. Akkari, C. B. Thompson, J. A. Joyce, and J. B. Xavier, "Metabolic origins of spatial organization in the tumor microenvironment," *Proc. Natl. Acad. Sci. U.S.A.* **114**, 2934–2939 (2017).
- <sup>37</sup>M. Wu, R.-Q. Su, X.-H. Li, T. Ellis, Y.-C. Lai, and X. Wang, "Engineering of regulated stochastic cell fate determination," *Proc. Natl. Acad. Sci. U.S.A.* **110**, 10610–10615 (2013).
- <sup>38</sup>L.-Z. Wang, R.-Q. Su, Z.-G. Huang, X. Wang, W.-X. Wang, C. Grebogi, and Y.-C. Lai, "A geometrical approach to control and controllability of nonlinear dynamical networks," *Nat. Commun.* **7**, 11323 (2016).
- <sup>39</sup>F.-Q. Wu, R.-Q. Su, Y.-C. Lai, and X. Wang, "Engineering of a synthetic quadrastable gene network to approach Waddington landscape and cell fate determination," *eLife* **6**, e23702 (2017).
- <sup>40</sup>T. Zhang, P. Brazhnik, and J. J. Tyson, "Exploring mechanisms of the DNA-damage response: P53 pulses and their possible relevance to apoptosis," *Cell Cycle* **6**, 85–94 (2007).
- <sup>41</sup>X. Zhang, F. Liu, Z. Cheng, and W. Wang, "Cell fate decision mediated by p53 pulses," *Proc. Natl. Acad. Sci. U.S.A.* **106**, 12245–12250 (2009).
- <sup>42</sup>X. Zhang, F. Liu, and W. Wang, "Two-phase dynamics of p53 in the DNA damage response," *Proc. Natl. Acad. Sci. U.S.A.* **108**, 8990–8995 (2011).
- <sup>43</sup>M. A. Nieto, R. Y.-J. Huang, R. A. Jackson, and J. P. Thiery, "EMT: 2016," *Cell* **166**, 21–45 (2016).
- <sup>44</sup>T. Z. Tan, Q. H. Miow, R. Y. Huang, M. K. Wong, J. Ye, J. A. Lau, M. Wu, L. H. A. Hadi, R. Soong, M. Choolani *et al.*, "Functional genomics identifies five distinct molecular subtypes with clinical relevance and pathways for growth control in epithelial ovarian cancer," *EMBO Mol. Med.* **5**, 1051–1066 (2013).
- <sup>45</sup>T. Z. Tan, Q. H. Miow, Y. Miki, T. Noda, S. Mori, R. Y. Huang, and J. P. Thiery, "Epithelial-mesenchymal transition spectrum quantification and its efficacy in deciphering survival and drug responses of cancer patients," *EMBO Mol. Med.* **6**, 1279–1293 (2014).
- <sup>46</sup>J. Zhang, X. J. Tian, H. Zhang, Y. Teng, R. Li, F. Bai, S. Elankumaran, and J. Xing, "TGF- $\beta$ -induced epithelial-to-mesenchymal transition proceeds through stepwise activation of multiple feedback loops," *Sci. Signal.* **7**, ra91 (2014).
- <sup>47</sup>V. Kaufman, T. Mihajev, and B. Drossel, "Scaling in critical random Boolean networks," *Phys. Rev. E* **72**, 046124 (2005).